



Nanochemistry approach for the fabrication of Fe and N co-decorated biomass-derived activated carbon frameworks: a promising oxygen reduction reaction electrocatalyst in neutral media

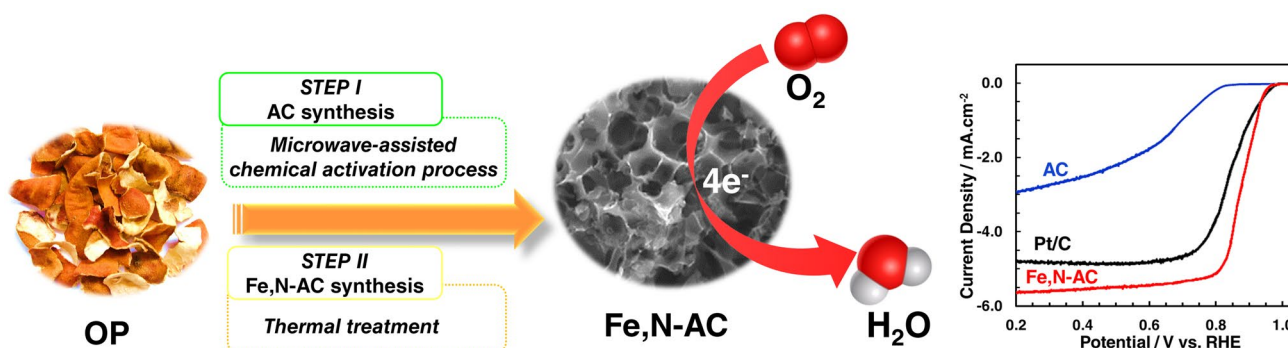
Hassan Karimi-Maleh¹ · Ceren Karaman² · Onur Karaman³ · Fatemeh Karimi⁴ · Yasser Vasseghian¹³ · Li Fu⁵ · Mehdi Baghayeri⁶ · Jalal Rouhi⁷ · P. Senthil Kumar⁸ · Pau-Loke Show⁹ · Saravanan Rajendran¹⁰ · Afsaneh L. Sanati¹¹ · Ali Mirabi¹²

Received: 27 January 2022 / Accepted: 3 March 2022 / Published online: 19 March 2022
© The Author(s), under exclusive licence to Islamic Azad University 2022

Abstract

The sluggish nature of the cathodic oxygen reduction reaction (ORR), and the expensive price of the precious metal-based nanocatalysts are the biggest obstacles to the practical applications of cutting-edge technologies including metal–air batteries and fuel cells. Hence, it is crucial to engineering a scalable-production pathway for the fabrication of a high-performance ORR catalyst. Herein, it was aimed to boost the performance of the ORR in neutral media, especially for microbial fuel cells, by tailoring a biomass-derived ORR electrocatalyst. In this regard, with the approach of nanochemistry, which is concerned with the fabrication of building blocks that vary in size, surface, shape, and defect characteristics, iron- and nitrogen-doped activated carbon framework (Fe,N-AC) was derived from waste orange peels by a two-stage pathway comprising microwave-assisted chemical activation and the thermal annealing processes. The physicochemical characterizations confirmed the successful co-doping of iron and nitrogen atoms to the activated carbon skeleton with the hierarchically ordered porous structure. Thanks to the interdependent effects of metal and heteroatoms in the structure, as well as the enlarged specific surface area ($1098 \text{ m}^2 \cdot \text{g}^{-1}$), Fe,N-AC catalyst offered a superior ORR activity thru the 4-electron transferring way ($n = 3.969$) with long-term stability (81.4% retention of initial current over the period of 7200 s). The half-wave potential was determined as 0.871 V by the introduction of iron and nitrogen to the nanoarchitecture, implying the boosting impact of the iron and nitrogen decoration. Moreover, the exceptional electrocatalytic activity of Fe,N-AC was validated by an onset potential of 0.951 V that was *ca.* 16 mV smaller than that of Pt/C catalyst (0.967 V). The accelerated S^{2-} poisoning test of Fe,N-AC catalyst was outperformed to Pt/C catalyst, thereby foreboding its practical utilization in MFCs. The current loss of Pt/C catalyst was determined almost five times that of Fe,N-AC catalyst at 5 mM S^{2-} concentration. The findings paved the course for the engineering of the state-of-the-art low-cost nanocatalyst by converting agricultural biomasses to a multi-functional advanced material to be employed in sustainable energy conversion systems.

Graphical abstract



Extended author information available on the last page of the article



Keywords Biomass · Oxygen reduction reaction · Neutral media · Iron and nitrogen doping · Activated carbon · Waste orange peel

Introduction

In addition to the outstanding efforts made for the utilization of green technologies to overcome the energy crisis, various subclasses of fuel cells (FCs) including direct alcohol FCs, microbial FCs, proton-exchange membrane FCs, etc., have been considered among the most promising alternative energy conversion systems owing to their superior advantages such as excellent efficiency and negligible greenhouse gas emission values [1–4]. Microbial fuel cells (MFCs), regarded as a viable prospect for renewable energy and green technology approaches, are the contemporary energy conversion systems that generate power via electrochemically microorganisms to catalyze the decomposition of biodegradable organic wastes [5]. In the cathode of the microbial fuel cells (MFCs), the oxygen reduction reaction (ORR) occurs, and its slow reaction kinetics hinders mainly the whole performance of the cell [6, 7]. Although noble metal-based electrocatalysts, especially Platinum (Pt), have been widely employed in MFCs to boost the reaction kinetics, they suffer from poor stability and poisoning from toxic intermediates, as well as their high-cost accounting for over half of the entire price of the cell. [8, 9]. Hence, it is of substantial importance to boost the electrocatalytic performance of the nanocatalyst while lowering the cost of the cell [10]. Thanks to the state-of-the-art advancement in nanotechnology, accompanied by the fabrication of novel nanocomposites such as metal-based [11–14], polymeric-based [15, 16], carbon-based [17, 18], etc. they have been employed in distinct areas including energy storage and conversion systems [19–22], environmental implementations [23–27], electrochemical (bio)sensors [28–32], pharmaceutical [33–36], antibacterial applications [37–39], (photo) catalysis [40, 41], etc.

Bimetallic or ternary nanocomposites fabricated by combining transition metals and noble metals have previously been reported to perform better [42, 43]. Furthermore, using a lower percentage of noble metal catalyst, the cost of the catalyst can be decreased. On the other hand, it is also possible to reduce the catalyst cost by designing noble metal-free electrocatalysts with high-catalytic activity, such as metal nitrides [44], metal/metal oxides [45, 46], metal chalcogenides, carbonaceous material supported metal catalysts [47], heteroatom-doped carbon structures, etc. [48–50]. Furthermore, noble metal-free nanocatalysts have recently garnered a lot of interest since they have a tolerance to toxic poisoning intermediates, are of relatively low price, and offer long-term operating stability [51, 52]. Additionally, amongst numerous carbon-based nanostructures, activated

carbon-based nanocatalysts have been regarded as one of the feasible nanocatalysts for ORR, thanks to their adjustable porous structure, tunable surface morphology, superior electrical conductivity, and a possibility to be synthesized from lignocellulosic agricultural wastes [53–57]. Processing of agricultural waste to a value-added material, namely activated carbon, is considered to be a promising way of waste management. However, there have been limited investigations on the tailoring of the agricultural waste-based activated carbons towards enhancing their ORR electrocatalytic activity and utilizing them in MFCs [58–60].

Surface engineering of the carbon-based materials with heteroatoms or metal nanoparticles can remarkably enhance their electrochemical activities thanks to enhanced electronic conductivity and increased number of electrochemically active sites [61]. Moreover, by accompanying the carbon skeleton it is possible to stabilize the metal nanoparticles, thereby improving the long-term stability of the electrocatalyst [51]. The synergistic influence of metal nanoparticles and heteroatoms doped onto high specific surface area carbon skeletons with high electrical conductivity is among the most well-known approaches of catalyst surface engineering [62].

With the above in mind, the fabrication of a cost-neutral high-performance ORR electrocatalyst that can be employed as a cathode catalyst in MFCs was aimed. It is worth noting that waste orange peels are a kind of lignocellulosic waste especially originated from in the juice beverages industry, thereby meaning it is of substantial potential for the engineering of carbon-based nanomaterials to be utilized in various applications. Considering this it was aimed to fabricate waste orange peel-derived activated carbon frameworks by microwave-assisted chemical activation process, followed by iron and nitrogen co-doping by thermal annealing process. Although up to now, the inclusion of both nitrogen and iron into various carbon architectures to fabricate an efficient ORR catalyst has been investigated [47, 63–65], to the based on the authors' information, this will be the first paper that investigates the ORR catalytic activity of the iron and nitrogen dual-decorated waste orange peel-derived activated carbon frameworks. The interdependent effect of dual decoration of nitrogen and iron nanoparticles on the electrocatalytic activity of biomass-derived carbon frameworks was highlighted in this study. Herein, it was desired to furnish a facile production pathway that meets the demands of sustainability and to engineer cost-effective functional nanocomposites with high electrocatalytic activity. In this regard, following the physicochemical characterization of the nanostructures, the electrochemical performance of the proposed

nanocatalyst towards ORR in alkaline media was explored through cyclic voltammetry (CV), linear sweep voltammetry (LSV), and chronoamperometry (CA) techniques. Moreover, the sulfide poison tolerances of the electrocatalysts were also investigated by CA measurement, as well as stability tests. The findings offered that the Fe,N-AC catalyst was capable of tremendously boosting the performance of the MFC in comparison to bare AC, and commercial Pt/C.

Experimental

Fabrication of AC

Activated carbon frameworks were fabricated by the thermal treatment procedure, following by microwave-assisted chemical activation of dried waste orange peels in the existence of H_3PO_4 . The collected waste orange peels were thoroughly scrubbed with a huge quantity of tap water, followed by deionized (DI) water, and allowed to dry in a vacuum oven at 80 °C until reached the constant weight [27]. Following that, the dried waste orange peels were crushed and sieved into a particle size ranging 250–500 μm and labeled as OP. Afterward, the acid washing pre-treatment was conducted. In this regard, 25 g of OP was introduced into a beaker containing 250 mL, 0.1 M HCl, and stirred at ambient temperature over 5 h. It was then filtered and rinsed with hot DI water until the pH reached 7.0. Then, the acid-washed OP was dried at 90 °C overnight and denoted as p-OP.

In the following step, a microwave-assisted chemical activation process was implemented in the existence of H_3PO_4 (85% wt.). As-obtained p-OP was coupled with a certain amount of H_3PO_4 (1:3 by weight), then placed into the Teflon-lined beaker, and allowed to impregnation of acid to the carbon precursor under stirring at ambient temperature for 72 h. Subsequently, the Teflon-lined beaker was placed into a microwave furnace and treated at 900 W, 2.45 GHz for 45 s. Followed by the microwave pre-treatment, the resultant sample was transferred into a quartz-tube furnace and the temperature was raised up to 450 °C (with a heating rate of 10 °C per minute) under a constant nitrogen gas flow rate, and it was maintained at this temperature over one hour. The resultant sample was bathed with hot water and then dried overnight at 80 °C. The eventual product was denoted as activated carbon (AC).

Fabrication of Fe,N-AC frameworks

The iron and nitrogen dual-decorated AC frameworks were synthesized by a facile thermal annealing process. In this regard, 1.0 g Iron(III) chloride was dispersed in 50 mL ethanol, followed by 50 mL ethylenediamine, as a nitrogen source, was introduced to the Iron(III) chloride–ethanol

dispersion to result in FeN_x species. Subsequently, 5.0 g of as-prepared AC was gently supplemented into the dispersion and continuously stirred over 24 h at 60 °C. Afterward, the resultant mixture, was placed into the vacuum oven and allowed to evaporate off the solvent at 90 °C. Following that, the obtained powder was thermally treated at 800 °C under nitrogen gas flow for over 1 h. Once the resultant sample cooled down to the ambient temperature, it was soaked into the 0.01 M HCl solution, followed by stirring over one hour to eliminate the residual iron species, filtered, and purged with deionized water until pH reached *ca.* 7.0. At last, it was allowed to dry at 80 °C over 24 h in a vacuum oven. The final sample was labeled as Fe,N-AC.

Physicochemical characterizations of nanostructures

The physicochemical features of as-synthesized nanostructures were characterized via field-emission scanning electron microscope (FESEM), transmission electron microscope (TEM), X-ray diffraction (XRD), N_2 adsorption–desorption isotherms, and X-ray photon spectrometer (XPS). Further information on the characterization techniques and the brands of each equipment were provided in the S.M. file.

Electrochemical characterization of nanostructures

The electrochemical characterizations of the catalysts were investigated in a typical three-electrode setup in which Pt-wire was employed as the counter electrode, whereas Ag/AgCl (3.0 M KCl) took role as reference electrode. The rotating disk electrode (RDE) modified by catalyst ink, on the other hand, was exploited as the working electrode. The details for the preparation of catalyst ink and electrode modification procedure were supplied in S.M.

The electrochemical analysis consisting of CV, LSV, and CA techniques were conducted on Gamry Reference 600 + workstation at ambient temperature. To assure the accuracy of the experiment, all electrochemical studies were carried out in triplicate. Moreover, by means of the Nernst Equation (see S.M. for details), all potentials in this work were normalized to a reversible hydrogen electrode (RHE).

The electrocatalytic features of the nanocatalysts towards ORR in neutral media were first assessed by CV responses in O_2 - and N_2 -saturated 0.1 mol.L⁻¹ phosphate buffered saline solution (PBS, pH = 7.0) electrolyte at room temperature, with a potential sweep rate of 15 mV.s⁻¹. LSV curves were recorded at varied rotational speeds ranging between 400 to 1600 rpm at 10 mV.s⁻¹. The number of transferred electron was computed with the help of the Koutecky–Levich model (the details are provided in S.M.).

The accelerated sulfur poisoning experiments were carried out by means of the chronoamperometry approach in



0.1 mol.L⁻¹ PBS at 0.1 V (vs. Ag/AgCl (3.0 M KCl)) in a typical 3-electrode cell as stated above. At the end of almost 60 min period of time when the stable current was acquired, Na₂S solutions with various concentrations ranging from 0.1 to 20.0 mM were introduced to the 0.1 mol.L⁻¹ PBS solution. After that, the normalized value of the current losses depending on the concentration of S²⁻ were plotted vs. time. Moreover, the stability of the as-synthesized electrocatalyst was explored by chronoamperometry analysis over a period of 7200 s at a rotational speed of 1600 rpm in O₂-saturated electrolytes.

Results and discussion

Evaluations of physicochemical characteristics of nanostructures

The SEM micrographs of the samples are illustrated in Fig. 1 to examine their morphology. The SEM of OP (Fig. 1A) implied the irregular bulk-surface structure formed by monolith plates with almost no holes/cavities possibly with a low specific surface area. The SEM images of p-OP (Fig. 1B) and AC (Fig. 1C), on the other hand, offered porous structure contributing to the increase in the specific surface area as a consequence of acid treatment and microwave-assisted activation steps. It was determined that p-OP was of a morphology that was uneven and heterogeneous on the surface (Fig. 1B), attributing to the fact that H₃PO₄ treatment

resulted in crumbly and rough surfaces as well as voids of various widths. At the end of microwave treatment, the surface of AC (Fig. 1C) became more regular with an ordered micro- and mesoporous structure, ascribed to the effect of microwave-assisted acid activation. The surface morphology of iron and nitrogen dual-decorated AC was explored by different magnification scanning electron microscopy images (Fig. 1D, E). A highly porous ordered carbon structure was observed, revealing its high specific surface area due to the increased active edges as a result of the iron and nitrogen doping process. It was obviously detected that the crater-like structures with thin walls were formed in the presence of iron and nitrogen species (Fig. 1E). The craters on the surfaces of carbons appear to be the consequence of the departing of phosphoric acid by evaporation from the space formerly filled by it, during the thermal treatment step [66]. TEM recordings were used to further investigate the morphology and architecture of the Fe,N-AC nanostructure (Fig. 1F). Several nanoparticles ranging in size between 5 and 30 nm were observed in the TEM micrograph of Fe,N-AC as shown in Fig. 1F.

The powdered X-ray spectrometry was performed in the 2θ range of 10°–90° to determine the crystalline nature of the Fe,N-AC nanostructure (Fig. 2A). The XRD spectra of Fe,N-AC offered the characteristic peaks of both carbon and zero-valent iron atom. The wide peak appeared at ca. 2θ = 24.4° was ascribed to the (002) crystalline plane of hexagonal structure carbonaceous materials [67], whereas the peaks detected at 2θ of ca. 44.8°, 65.1°, and 82.2° were

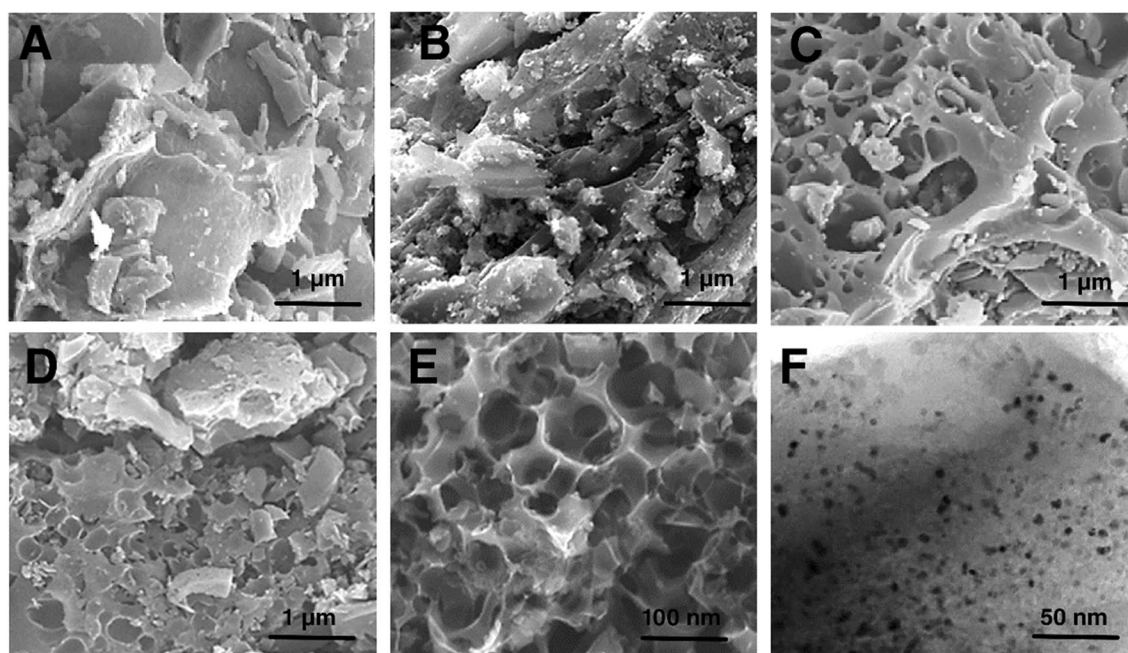


Fig. 1 The scanning electron microscopy images of **A** OP, **B** p-OP, **C** AC, and **D**, **E** Fe,N-AC, and **F** the transmission electron microscopy image of Fe,N-AC

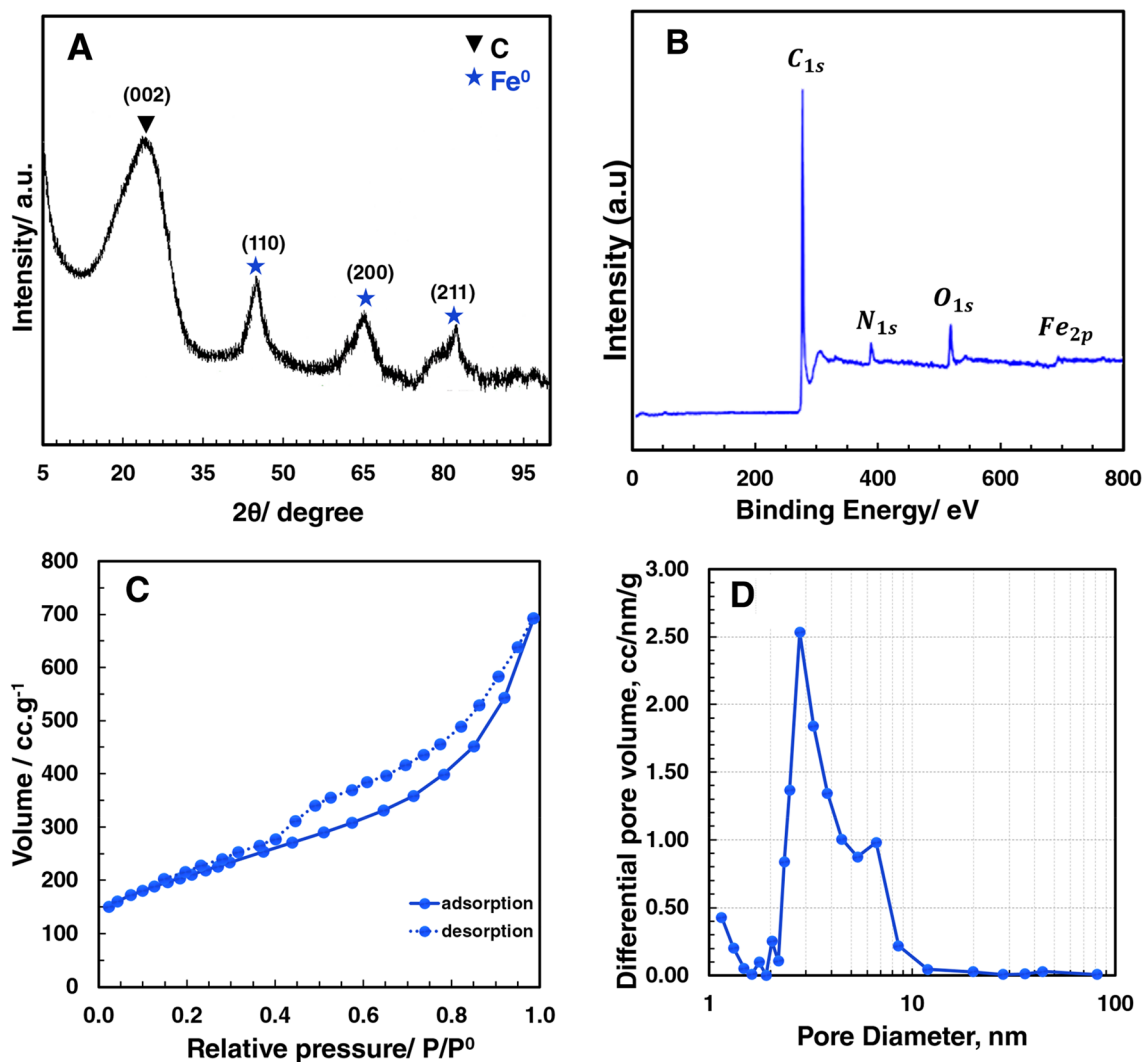


Fig. 2 **A** XRD pattern, **B** full range XPS survey, **C** nitrogen adsorption–desorption isotherm, **D** BJH pore size distribution curve of Fe,N-AC frameworks

ascribed to the (110), (200), and (211) planes of zero-valent iron atoms (JCPDS card #06-0696) [68, 69]. Moreover, for comparison, the XRD spectrum of waste orange peel-derived AC sample is presented in Fig. S1. The peaks that appeared at approximately $2\theta=24.2^\circ$ and 42.8° in the XRD diffraction pattern of the as-fabricated AC were assigned to the (002) and (100) facets of carbonaceous materials, respectively. The XRD spectra confirmed the successful synthesis of Fe,N-AC, as well as the purity of the nanostructure.

The full range XPS spectra of the Fe,N-AC frameworks are illustrated in Fig. 2B to explore and confirm the chemical composition of the structure. There was only C1s, N1s, O1s, and Fe2p peaks were detected in the full range XPS spectra at almost 284.9 eV, 398.2 eV, 530.6 eV, and 710.7 eV, respectively. The XPS survey demonstrated the effective

integration of nitrogen and iron atoms into the activated carbon frameworks, as well as the nanostructure's purity.

The specific surface area and PSD curve of as-synthesized AC and Fe,N-AC frameworks were explored by nitrogen adsorption–desorption investigations. The BJH curve and the BET isotherm of AC sample were also provided in Fig. S2. The results demonstrated that the nitrogen adsorption–desorption isotherm of AC corresponded to the type IV isotherm with the H4 hysteresis loop, which was attributed to the thin slit-like organized micro- and mesopores [70]. The specific surface area of AC sample was obtained as $1019\text{ m}^2\cdot\text{g}^{-1}$ according to BET analysis. The total pore volume of AC was determined as $0.418\text{ cc}\cdot\text{g}^{-1}$, and the BJH curves of bare AC sample confirmed the formation of ordered micro- and mesopores which were in accordance with SEM images.



The BET surface area of the Fe,N-AC was computed as $ca. 1098 \text{ m}^2 \cdot \text{g}^{-1}$ with the help of N_2 adsorption–desorption isotherm (Fig. 2C), which was well-suited to the type IV isotherm having a hysteresis loop of H3 type, displaying the micro- and mesoporous besides the tiny macropores. The findings were in accordance with the scanning electron micrographs of the Fe,N-AC. The BJH pore size distribution curve (Fig. 2D) confirmed the ordered micro- and mesoporous structures with a cumulative adsorption pore volume of $0.986 \text{ cc} \cdot \text{g}^{-1}$. It was expected that thanks to the large pore volume and the high specific surface area, the electrocatalytic performance would be facilitated by permitting the easy transfer of the ions throughout the pore channels with lowered charge transfer resistance.

Evaluations of electrocatalytic performance of Fe,N-AC frameworks

The ORR activity of Fe,N-AC frameworks was explored first by CV experiments at $15 \text{ mV} \cdot \text{s}^{-1}$ scan rate in N_2 - and O_2 -saturated neutral electrolyte of PBS (Fig. 3A). Although there was no visible peak detected in the nitrogen-saturated electrolyte, the significant peak appeared at $ca. 0.850 \text{ V}$ in oxygen-saturated electrolyte for Fe,N-AC revealed its electrocatalytic activity towards ORR (Fig. 3A). The potential of the reduction peak was determined so closed to the Pt/C electrocatalyst (0.853 V). The hump observed at anodic CV scan of Fe,N-AC in the O_2 -saturated electrolyte was ascribed to the pseudocapacitive effect of both Fe nanoparticles and N atoms. It was revealed that the bare AC framework, on the other hand, was of a negligible catalytic activity since there

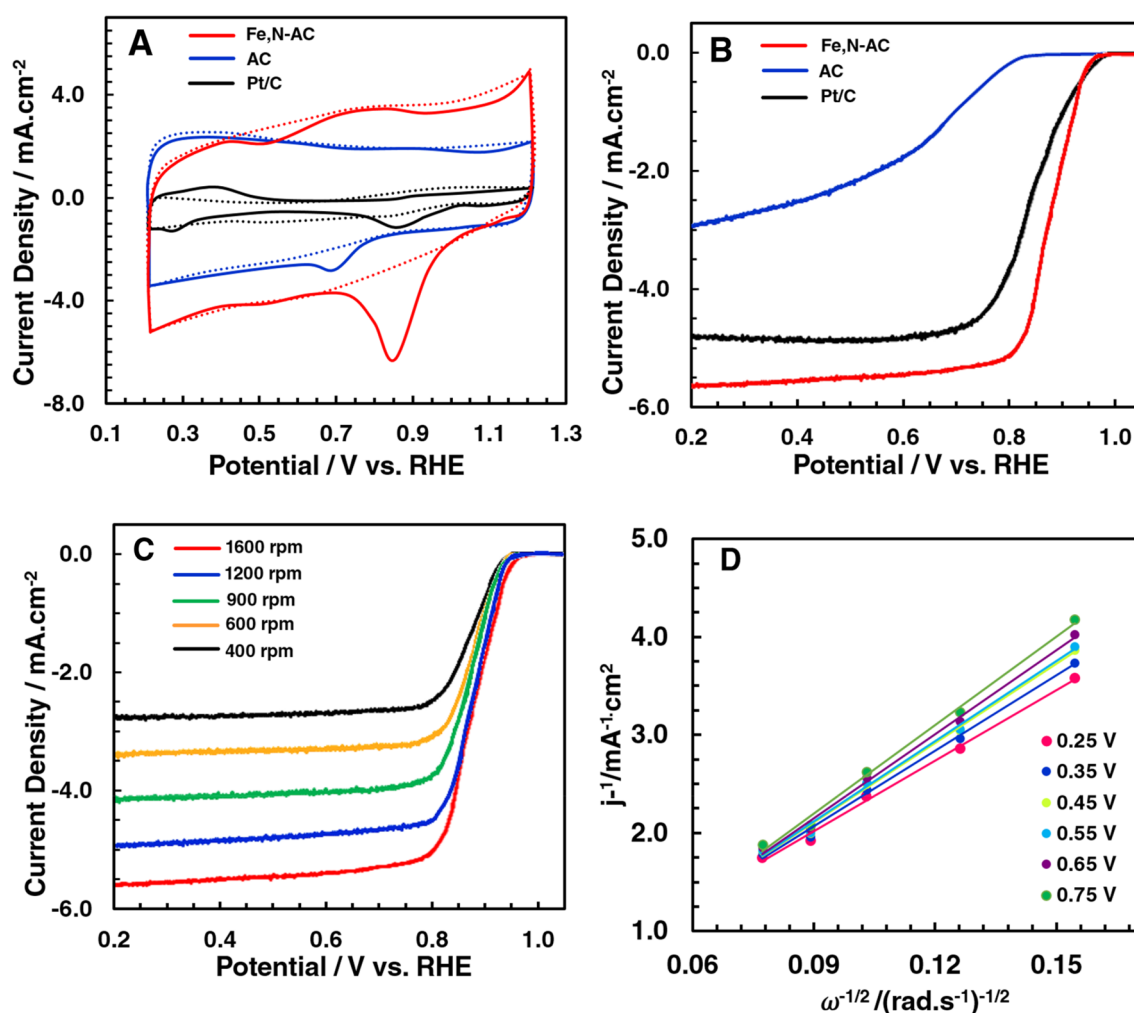


Fig. 3 **A** Cyclic voltammograms of nanocatalysts recorded in N_2 (dashed lines)- and O_2 (solid lines)-saturated $0.1 \text{ mol} \cdot \text{L}^{-1}$ PBS electrolyte ($\text{pH}=7$) at $15 \text{ mV} \cdot \text{s}^{-1}$; LSV polarization curves of **(B)**. All nanocatalysts at a rotation speed of 1600 rpm , and **C** Fe,N-AC elec-

trocatalyst at different rotation speed ranging $400\text{--}1600 \text{ rpm}$ in oxygenated $0.1 \text{ mol} \cdot \text{L}^{-1}$ PBS electrolyte ($\text{pH}=7$); **D** The Koutecky–Levich plots of Fe,N-AC electrocatalyst at different potentials

was a slight oxygen reduction peak observed at *ca.* 0.698 V (Fig. 3A). Moreover, in comparison to the CV curves in oxygen-saturated electrolyte for bare AC network, it was obviously concluded that the inclusion of iron and nitrogen species into the structure endowed the electrocatalytic activity towards ORR. However, it would be better to mention that both Fe,N-AC and bare AC were of capacitive behavior, confirmed by a semi-rectangular CV curve with high current density values. As a result, these results illustrated that Fe,N-AC framework would have a low overpotential and enhanced ORR catalytic activity.

Moreover, to assess the catalytic activity LSV curves of catalysts were acquired a rotational rate of 1600 rpm in oxygenated electrolyte and compared (Fig. 3B). Although the LSV curve of bare AC revealed nearly no ORR activity, effective ORR electrocatalytic activity of Fe,N-AC with a $4e^-$ transfer way was affirmed by a well-defined diffusion plateau. The half-wave potential ($E_{1/2}$) value of bare AC boosted almost 1.2-fold and reached 0.871 V with the introduction of iron and nitrogen to the structure, implying the boosting impact of the iron nanoparticles and nitrogen atoms (Fig. 3B). The $E_{1/2}$ value of Pt/C, on the other hand, was determined to be 0.852 V at the same condition. Moreover, the outstanding electrocatalytic performance of Fe,N-AC nanocatalyst was also proved with the onset potential (E_{onset}) of 0.951 V which was only *ca.* 16 mV lower than that of Pt/C (0.967 V). These findings were promising in comparison to other reported ORR electrocatalysts for neutral media and offered the remarkable superiority of the synthesized nanocatalysts [71–77].

The linear sweep voltammograms of Fe,N-AC catalyst obtained at varying rotational speeds in oxygenated electrolyte were presented in Fig. 3C. High rotation speeds result in instantaneous transportation of the oxygen molecules to the electrode surface and, as a result, higher diffusion limiting current densities (j_L) could be achieved as rotation speeds increase due to the shorter diffusion distance. It was confirmed with the help of K-L plots (Fig. 3D) extracted from linear sweep voltammetry curves at varied rotational rates that the Fe,N-AC electrocatalyst catalyzed the ORR occurred through the $4e^-$ transfer mechanism ($n = 3.969$). In comparison, the n value for the bare AC catalyst was also computed as 2.73, indicating that bare AC might catalyze oxygen reduction reaction via a direct $2e^-$ pathway with a high peroxide yield [78]. Hence, it can be speculated that

introducing iron and nitrogen atoms to the AC framework facilitates the reduction of O_2 molecules to H_2O molecules via the $4e^-$ transfer mechanism [79]. The various iron–nitrogen-doped carbonaceous neutral media ORR electrocatalysts were compared in Table S1. The reported values of electron transfer numbers offered that the as-synthesized Fe,N-AC was of superior to or comparable performance with the similar electrocatalysts.

The obtained parameters related to the electrocatalytic features of nanocatalyst towards the ORR were tabulated in Table 1. Although the sluggish reaction kinetics of oxygen reduction at bare AC, these findings indicated that the presence of iron and nitrogen atoms can significantly boost the intrinsic activity of Fe,N-AC. Additionally, it is worth noting that the charge/spin distribution caused by nitrogen doping is mostly responsible for the electrocatalytic activity of carbonaceous nanocatalyst [80]. The presence of large mesoporous also aided the oxygen transportation, and a certain amount of micropores on the Fe,N-AC frameworks also boosted the electrochemically active sites. In brief, thanks to the prevention of aggregation of iron nanoparticles, enhancing the electrochemically active sites, the ordered porous carbon structure with high specific surface area derived from agricultural waste, and the contribution of nitrogen-comprising surface functionalities, the ORR performance was significantly boosted.

The sulfide/sulfate ion poisoning of the Pt catalyst is another critical constraint to consider in the actual implementation of microbial fuel cells. S^{2-} and SO_4^{2-} , two typical wastewater components, are known to reduce Pt electrocatalytic activity in microbial fuel cells [81, 82]. Hence, the poisoning tolerance of Fe,N-AC was assessed by the divergence between the initial current and the current obtained after injecting the S^{2-} species at a specific concentration. The current losses were computed as a function of the S^{2-} concentration as well (Fig. 4A). The current loss of Pt/C catalyst was *ca.* 5 folds of that of Fe,N-AC catalyst at an S^{2-} concentration of 5 mM. These findings corroborated the findings of the chronoamperometry studies (Fig. 4B) performed to evaluate the catalyst's stability. The Fe,N-AC catalyst preserved 81.4% of its initial catalytic activity, whereas that was determined only 65.1% for Pt/C catalyst. Pt/C swiftly lost its initial activity, attributed to its poor tolerance for toxic S^{2-} species, and performed poorly when compared to Fe, N-AC. These experiments revealed that the Fe,N-AC

Table 1 The comparison of electrocatalytic performance parameters of as-synthesized nanocatalysts

Catalyst	ORR peak potential (V vs. RHE)	E_{onset} (V vs. RHE)	$E_{1/2}$ (V vs. RHE)	n_{average}	j_L (mA.cm ⁻²)
AC	0.698	0.801	0.724	3.73	–2.98
Pt/C	0.853	0.967	0.850	3.996	–4.71
Fe,N-AC	0.850	0.951	0.870	3.969	–5.58



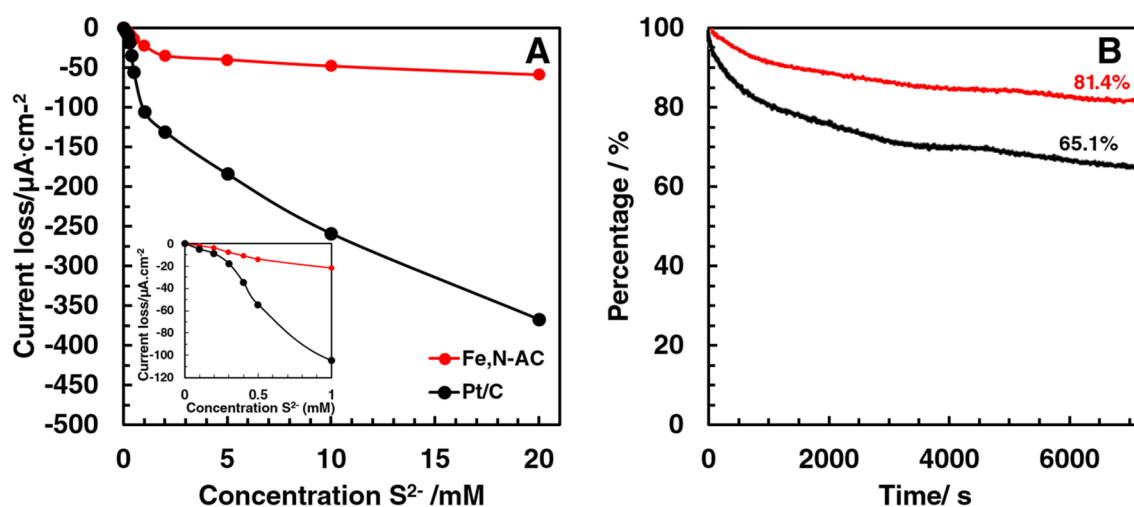


Fig. 4 **A** Recorded current losses vs. the concentration of S^{2-} introduced to the electrolyte media; **B** Chronoamperometry curves of Fe,N-AC and Pt/C over the time period of 7200 s

framework had significantly superior poisoning tolerance and long-term durability than Pt/C in the same microbial fuel cell operating conditions.

Conclusions

Herein, a simple and sustainable fabrication pathway to the engineering iron- and nitrogen-doped activated carbon from waste orange peels with a nanochemistry approach was proposed. The synthesized Fe,N-AC frameworks were assessed to be employed as a possible ORR electrocatalyst for the MFCs. The electroactivity of waste orange peel-derived AC catalyst towards ORR in neutral media was considerably boosted by the dual decoration of zero-valent iron nanoparticles and nitrogen atoms to the nanostructure. This phenomenon was linked to the lowering of diffusion resistance and charge transfer resistance thanks to the enlarged BET surface area of $1098 \text{ m}^2\cdot\text{g}^{-1}$, comprising of abundant micro- and mesopores, as well as the interdependent effect of the Fe nanoparticles and N atoms. The ORR mechanism was altered from the $2e^-$ pathway ($n = 2.73$ for bare AC) to the $4e^-$ mechanism ($n = 3.969$ for Fe,N-AC), thanks to the superior electrochemical features of Fe,N-AC framework with abundant electrochemically active sites. The improved activity of fabricated Fe,N-AC catalyst was further validated by its E_{onset} value of 0.951 V, that was only about 16 mV smaller than that of Pt/C ($E_{\text{onset}} = 0.967 \text{ V}$). The high specific surface area of waste orange peel-derived activated carbon frameworks allowed metal nanoparticles to disperse uniformly without aggregation, thereby enhancing the electrocatalytic activity. In comparison to conventional Pt/C catalyst, the Fe,N-AC frameworks offered exceptional

tolerance to poisonous S^{2-} contaminants, besides its superior stability (81.4% over the period of 7200 s). The employment of the as-synthesized Fe,N-AC as a cathode catalyst can, thus, significantly facilitate power generation in MFCs, and also its application in microbial fuel cells for wastewater treatment should be possible, thanks to its superior tolerance to poisoning species. In brief, this work could open up a viable route for catalyst engineering of low-cost ORR electrocatalysts from sustainable biomass precursors, together with outstanding catalytic activity.

Supplementary Information The online version contains supplementary material available at <https://doi.org/10.1007/s40097-022-00492-3>.

References

- Burhan, H., Arikan, K., Alma, M.H., Nas, M.S., Karimi-Maleh, H.Ş., Karimi, F., Vasseghian, Y.: Highly efficient carbon hybrid supported catalysts using nano-architecture as anode catalysts for direct methanol fuel cells. *Int. J. Hydro. Energy* (2022). <https://doi.org/10.1016/j.ijhydene.2021.12.141>
- Dasdelen, Z., Yildiz, Y., Eris, S., Sen, F.: Enhanced electrocatalytic activity and durability of Pt nanoparticles decorated on GO-PVP hybride material for methanol oxidation reaction. *Appl. Catal. B-Environ.* **219**, 511–516 (2017)
- Eris, S., Dasdelen, Z., Sen, F.: Enhanced electrocatalytic activity and stability of monodisperse Pt nanocomposites for direct methanol fuel cells. *J. Colloid. Interf. Sci.* **513**, 767–773 (2018)
- Taherian, Z., Khataee, A., Han, N., Orooji, Y.: Hydrogen production through methane reforming processes using promoted-Ni/mesoporous silica: a review. *J. Ind. Eng. Chem.* **107**, 20–30 (2022)
- Kannan, M.V., Kumar, G.G.: Current status, key challenges and its solutions in the design and development of graphene based ORR catalysts for the microbial fuel cell applications. *Biosens. Bioelectron.* **77**, 1208–1220 (2016)

6. Mahalingam, S., Ayyaru, S., Ahn, Y.H.: Enhanced cathode performance of Fe₂O₃, boron nitride-doped rGO nanosheets for microbial fuel cell applications. *Sustain. Energy Fuels*. **4**(3), 1454–1468 (2020)
7. Zhao, F., Harnisch, F., Schröder, U., Scholz, F., Bogdanoff, P., Herrmann, I.: Challenges and constraints of using oxygen cathodes in microbial fuel cells. *Environ. Sci. Technol.* **40**(17), 5193–5199 (2006)
8. Yuan, H.Y., Hou, Y., Abu-Reesh, I.M., Chen, J.H., He, Z.: Oxygen reduction reaction catalysts used in microbial fuel cells for energy-efficient wastewater treatment: a review. *Mater. Horiz.* **3**(5), 382–401 (2016)
9. Rozendal, R.A., Hamelers, H.V.M., Rabaey, K., Keller, J., Buisman, C.J.N.: Towards practical implementation of bioelectrochemical wastewater treatment. *Trends Biotechnol.* **26**(8), 450–459 (2008)
10. Steele, B.C.H., Heinzl, A.: Materials for fuel-cell technologies. *Nature* **414**(6861), 345–352 (2001)
11. Zhang, H., Jiang, J., Li, J., Li, Y., Zhou, L., Gao, H., Liu, S.: Preparation and properties of TiO₂/chitosan/acrylic acid in situ cross-linked composite hydrogel. *J. Forest. Eng.* **5**, 76–81 (2020)
12. Zhang, Y., Wei, L., Lu, L., Gan, L., Mingzhu, P.: Adsorption-photocatalytic properties of cellulose nanocrystal supported ZnO nanocomposites. *J. Forest. Eng.* **5**, 29–35 (2020)
13. Cheng, Z., Meng, J., Wang, X.: Preparation of wood-based filter loaded with Ag nanoparticles and its catalytic degradation performance on organic dye. *J. Forest. Eng.* **5**(6), 94–98 (2020)
14. Taherian, Z., Shahed Gharahshiran, V., Khataee, A., Orooji, Y.: Synergistic effect of freeze-drying and promoters on the catalytic performance of Ni/MgAl layered double hydroxide. *Fule* **311**, 122620 (2022)
15. Deeksha, B., Sadanand, V., Hariram, N., Rajulu, A.V.: Preparation and properties of cellulose nanocomposite fabrics with in situ generated silver nanoparticles by bioreduction method. *J. Bioresour. Bioprod.* **6**(1), 75–81 (2021)
16. Joseph, B., Sagarika, V.K., Sabu, C., Kalarikkal, N., Thomas, S.: Cellulose nanocomposites: fabrication and biomedical applications. *J. Bioresour. Bioprod.* **5**(4), 223–237 (2020)
17. Qian, H., Wang, J., Yan, L.: Synthesis of lignin-poly(*N*-methylaniline)-reduced graphene oxide hydrogel for organic dye and lead ions removal. *J. Bioresour. Bioprod.* **5**(3), 204–210 (2020)
18. Arefi-Oskoui, S., Khataee, A., Behrouz, S.J., Vatanpour, V., Gharamaleki, S.H., Orooji, Y., Safarpour, M.: Development of MoS₂/O-MWCNTs/PES blended membrane for efficient removal of dyes, antibiotic, and protein. *Sep. Purif. Technol.* **280**, 119822 (2022)
19. Korkmaz, S., Kariper, I.A., Karaman, O., Karaman, C.: The production of rGO/ RuO₂ aerogel supercapacitor and analysis of its electrochemical performances. *Ceram Int.* **47**(24), 34514–34520 (2021)
20. Akca, A., Karaman, O., Karaman, C.: Mechanistic insights into catalytic reduction of N₂O by CO over Cu-embedded graphene: a density functional theory perspective. *ECS J. Solid State Sci.* **10**(4), 041003 (2021)
21. Karimi, F., Ghorbani, M., Lashkenari, M.S., Jajroodi, M., Talooki, E.F., Vaseghian, Y., Karaman, O., Karaman, C.: Polyaniline-manganese ferrite supported platinum-ruthenium nanohybrid electrocatalyst: synergizing tailoring toward boosted ethanol oxidation reaction. *Top. Catal.* (2021). <https://doi.org/10.1007/s11244-021-01537-7>
22. Alamgholiloo, H., Rostamnia, S., Hassankhani, A., Liu, X., Eftekhari, A., Hasanzadeh, A., Zhang, K., Karimi-Maleh, H., Khaksar, S., Varma, R.S., Shokouhimehr, M.: Formation and stabilization of colloidal ultra-small palladium nanoparticles on diamine-modified Cr-MIL-101: synergic boost to hydrogen production from formic acid. *J. Colloid. Interf. Sci.* **567**, 126–135 (2020)
23. Karimi, F., Ayati, A., Tanhaei, B., Sanati, A.L., Afshar, S., Kardan, A., Dabirifar, Z., Karaman, C.: Removal of metal ions using a new magnetic chitosan nano-bio-adsorbent; a powerful approach in water treatment. *Environ. Res.* **203**, 111753 (2022)
24. Al Sharabati, M., Abokwiek, R., Al-Othman, A., Tawalbeh, M., Karaman, C., Orooji, Y., Karimi, F.: Biodegradable polymers and their nano-composites for the removal of endocrine-disrupting chemicals (EDCs) from wastewater: a review. *Environ Res.* **202**, 111694 (2021)
25. Rajendran, S., Priya, T.A.K., Khoo, K.S., Hoang, T.K.A., Ng, H.S., Munawaroh, H.S.H., Karaman, C., Orooji, Y., Show, P.L.: A critical review on various remediation approaches for heavy metal contaminants removal from contaminated soils. *Chemosphere* **287**, 132369 (2022)
26. Karaman, C., Karaman, O., Show, P.L., Orooji, Y., Karimi-Maleh, H.: Utilization of a double-cross-linked amino-functionalized three-dimensional graphene networks as a monolithic adsorbent for methyl orange removal: equilibrium, kinetics, thermodynamics and artificial neural network modeling. *Environ. Res.* **207**, 1121156 (2021)
27. Karaman, C., Karaman, O., Show, P.L., Karimi-Maleh, H., Zare, N.: Congo red dye removal from aqueous environment by cationic surfactant modified-biomass derived carbon: equilibrium, kinetic, and thermodynamic modeling, and forecasting via artificial neural network approach. *Chemosphere* **290**, 133346 (2021)
28. Karimi-Maleh, H., Karimi, F., Fu, L., Sanati, A.L., Alizadeh, M., Karaman, C., Orooji, Y.: Cyanazine herbicide monitoring as a hazardous substance by a DNA nanostructure biosensor. *J. Hazard Mater.* **423**, 127058 (2022)
29. Karimi-Maleh, H., Khataee, A., Karimi, F., Baghayeri, M., Fu, L., Rouhi, J., Karaman, C., Karaman, O., Boukherroub, R.: A green and sensitive guanine-based DNA biosensor for idarubicin anticancer monitoring in biological samples: a simple and fast strategy for control of health quality in chemotherapy procedure confirmed by docking investigation. *Chemosphere* **291**, 132928 (2021)
30. Karimi-Maleh, H., Ahanjan, K., Taghavi, M., Ghaemy, M.: A novel voltammetric sensor employing zinc oxide nanoparticles and a new ferrocene-derivative modified carbon paste electrode for determination of captopril in drug samples. *Anal. Methods-UK* **8**(8), 1780–1788 (2016)
31. Mohanraj, J., Durgalakshmi, D., Rakkesh, R.A., Balakumar, S., Rajendran, S., Karimi-Maleh, H.: Facile synthesis of paper based graphene electrodes for point of care devices: a double stranded DNA (dsDNA) biosensor. *J. Colloid. Interf. Sci.* **566**, 463–472 (2020)
32. Sohrabi, H., Majidi, M.R., Arbabzadeh, O., Khaaki, P., Pourmohammad, S., Khataee, A., Orooji, Y.: Recent advances in the highly sensitive determination of zearalenone residues in water and environmental resources with electrochemical biosensors. *Environ. Res.* **204**, 112082 (2022)
33. Cheraghi, S., Taher, M.A., Karimi-Maleh, H.: A novel strategy for determination of paracetamol in the presence of morphine using a carbon paste electrode modified with CdO nanoparticles and ionic liquids. *Electroanal.* **28**(2), 366–371 (2016)
34. Alavi-Tabari, S.A.R., Khalilzadeh, M.A., Karimi-Maleh, H.: Simultaneous determination of doxorubicin and dasatinib as two breast anticancer drugs uses an amplified sensor with ionic liquid and ZnO nanoparticle. *J. Electroanal. Chem.* **811**, 84–88 (2018)
35. Taherkhani, A., Jamali, T., Hadadzadeh, H., Karimi-Maleh, H., Beitollahi, H., Taghavi, M., Karimi, F.: ZnO nanoparticle-modified ionic liquid-carbon paste electrode for voltammetric determination of folic acid in food and pharmaceutical samples. *Ionics* **20**(3), 421–429 (2014)




36. Hojjati-Najafabadi, A., Salmanpour, S., Sen, F., Asrami, P.N., Mahdavian, M., Khalilzadeh, M.A.: A tramadol drug electrochemical sensor amplified by biosynthesized Au nanoparticle using *Mentha aquatic* extract and ionic liquid. *Top. Catal.* (2021). <https://doi.org/10.1007/s11244-021-01498-x>
37. Mansoorianfar, M., Shahin, K., Hojjati-Najafabadi, A., Pei, R.: MXene–laden bacteriophage: a new antibacterial candidate to control bacterial contamination in water. *Chemosphere* **290**, 133383 (2022)
38. Hojjati-Najafabadi, A., Davar, F., Enteshari, Z., Hosseini-Koupaei, M.: Antibacterial and photocatalytic behaviour of green synthesis of Zn_{0.95}Ag_{0.05}O nanoparticles using herbal medicine extract. *Ceram Int.* **47**(22), 31617–31624 (2021)
39. Torkian, N., Bahrami, A., Hosseini-Abari, A., Momeni, M.M., Abdolkarimi-Mahabadi, M., Bayat, A., Hajipour, P., Rourani, H.A., Abbasi, M.S., Torkian, S., Wen, Y.: Synthesis and characterization of Ag-ion-exchanged zeolite/TiO₂ nanocomposites for antibacterial applications and photocatalytic degradation of antibiotics. *Environ. Res.* **207**, 112157 (2021)
40. Akhoondi, A., Feleni, U., Bethi, B., Idris, A.O., Hojjati-Najafabadi, A.: Advances in metal-based vanadate compound photocatalysts: synthesis, properties and applications. *Synthesis Sinter.* **1**(3), 151–168 (2021)
41. Keyikoglu, R., Khataee, A., Lin, H., Orooji, Y.: Vanadium (V)-doped ZnFe LDH for enhanced sonocatalytic degradation of pymetrozine. *Chem. Eng. J.* **434**, 134730 (2022)
42. Yang, H.Z., Zhang, J., Sun, K., Zou, S.Z., Fang, J.Y.: Enhancing by weakening: electrooxidation of methanol on Pt₃Co and Pt nanocubes. *Angew. Chem. Int. Edit.* **49**(38), 6848–6851 (2010)
43. Stamenkovic, V.R., Fowler, B., Mun, B.S., Wang, G.F., Ross, P.N., Lucas, C.A., Markovic, N.M.: Improved oxygen reduction activity on Pt₃Ni(111) via increased surface site availability. *Science* **315**(5811), 493–497 (2007)
44. Wu, H.B., Chen, W.: Copper nitride nanocubes: size-controlled synthesis and application as cathode catalyst in alkaline fuel cells. *J. Am. Chem. Soc.* **133**(39), 15236–15239 (2011)
45. Liang, Y.Y., Wang, H.L., Diao, P., Chang, W., Hong, G.S., Li, Y.G., Gong, M., Xie, L.M., Zhou, J.G., Wang, J., Regier, T.Z., Wei, F., Dai, H.J.: Oxygen reduction electrocatalyst based on strongly coupled cobalt oxide nanocrystals and carbon nanotubes. *J. Am. Chem. Soc.* **134**(38), 15849–15857 (2012)
46. Yin, H.J., Tang, H.J., Wang, D., Gao, Y., Tang, Z.Y.: Facile synthesis of surfactant-free Au cluster/graphene hybrids for high-performance oxygen reduction reaction. *ACS Nano* **6**(9), 8288–8297 (2012)
47. Lefevre, M., Proietti, E., Jaouen, F., Dodelet, J.P.: Iron-based catalysts with improved oxygen reduction activity in polymer electrolyte fuel cells. *Science* **324**(5923), 71–74 (2009)
48. Zhang, L., Zhang, J.J., Wilkinson, D.P., Wang, H.J.: Progress in preparation of non-noble electrocatalysts for PEM fuel cell reactions. *J. Power Sources* **156**(2), 171–182 (2006)
49. Gong, K.P., Du, F., Xia, Z.H., Durstock, M., Dai, L.M.: Nitrogen-doped carbon nanotube arrays with high electrocatalytic activity for oxygen reduction. *Science* **323**(5915), 760–764 (2009)
50. Karaman, C.: Boosting effect of nitrogen and phosphorous co-doped three-dimensional graphene architecture: highly selective electrocatalysts for carbon dioxide electroreduction to formate. *Top. Catal.* (2021). <https://doi.org/10.1007/s11244-021-01500-6>
51. Karaman, O.: Oxygen reduction reaction performance boosting effect of nitrogen/sulfur co-doped graphene supported cobalt phosphide nanoelectrocatalyst: pH-universal electrocatalyst. *ECS J. Solid State Sci.* **10**(6), 061003 (2021)
52. Yuan, Y., Yuan, T., Wang, D.M., Tang, J.H., Zhou, S.G.: Sewage sludge biochar as an efficient catalyst for oxygen reduction reaction in a microbial fuel cell. *Bioresour. Technol.* **144**, 115–120 (2013)
53. Xu, G.Y., Han, J.P., Ding, B., Nie, P., Pan, J., Dou, H., Li, H.S., Zhang, X.G.: Biomass-derived porous carbon materials with sulfur and nitrogen dual-doping for energy storage. *Green Chem.* **17**(3), 1668–1674 (2015)
54. Sudhan, N., Subramani, K., Karnan, M., Ilayaraja, N., Sathish, M.: Biomass-derived activated porous carbon from rice straw for a high-energy symmetric supercapacitor in aqueous and non-aqueous electrolytes. *Energy Fuel.* **31**(1), 977–985 (2017)
55. Chaitra, K., Vinny, R.T., Sivaraman, P., Reddy, N., Hu, C.Y., Venkatesh, K., Vivek, C.S., Nagaraju, N., Kathyayini, N.: KOH activated carbon derived from biomass-banana fibers as an efficient negative electrode in high performance asymmetric supercapacitor. *J. Energy Chem.* **26**(1), 56–62 (2017)
56. Ma, G.F., Yang, Q., Sun, K.J., Peng, H., Ran, F.T., Zhao, X.L., Lei, Z.Q.: Nitrogen-doped porous carbon derived from biomass waste for high-performance supercapacitor. *Bioresour. Technol.* **197**, 137–142 (2015)
57. Ma, G.F., Tang, W., Sun, K.J., Zhang, Z.G., Feng, E.K., Lei, Z.Q.: Coprinus comatus-based nitrogen-doped active carbon for high performance supercapacitor. *NANO* **12**(8), 1750103 (2017)
58. Li, S.N., Ho, S.H., Hua, T., Zhou, Q.X., Li, F.X., Tang, J.C.: Sustainable biochar as an electrocatalysts for the oxygen reduction reaction in microbial fuel cells. *Green Energy Environ.* **6**(5), 644–659 (2021)
59. Huggins, T.M., Pietron, J.J., Wang, H.M., Ren, Z.J., Biffinger, J.C.: Graphitic biochar as a cathode electrocatalyst support for microbial fuel cells. *Bioresour. Technol.* **195**, 147–153 (2015)
60. Chakraborty, I., Sathe, S.M., Dubey, B.K., Ghangrekar, M.M.: Waste-derived biochar: applications and future perspective in microbial fuel cells. *Bioresour. Technol.* **312**, 123587 (2020)
61. Karaman, C., Bayram, E., Karaman, O., Aktas, Z.: Preparation of high surface area nitrogen doped graphene for the assessment of morphologic properties and nitrogen content impacts on supercapacitors. *J. Electroanal. Chem.* **868**, 114197 (2020)
62. Sun, M., Davenport, D., Liu, H.J., Qu, J.H., Elimelech, M., Li, J.H.: Highly efficient and sustainable non-precious-metal Fe-N-C electrocatalysts for the oxygen reduction reaction. *J. Mater. Chem. A.* **6**(6), 2527–2539 (2018)
63. Xiao, H., Shao, Z.G., Zhang, G., Gao, Y., Lu, W.T., Yi, B.L.: Fe-N-carbon black for the oxygen reduction reaction in sulfuric acid. *Carbon* **57**, 443–451 (2013)
64. Pan, Y.J., Mo, X.P., Li, K.X., Pu, L.T., Liu, D., Yang, T.T.: Iron-nitrogen-activated carbon as cathode catalyst to improve the power generation of single-chamber air-cathode microbial fuel cells. *Bioresour. Technol.* **206**, 285–289 (2016)
65. Yang, W.L., Logan, B.E.: Immobilization of a metal-nitrogen-carbon catalyst on activated carbon with enhanced cathode performance in microbial fuel cells. *Chemosuschem* **9**(16), 2226–2232 (2016)
66. Prahas, D., Kartika, Y., Indraswati, N., Ismadji, S.: Activated carbon from jackfruit peel waste by H₃PO₄ chemical activation: pore structure and surface chemistry characterization. *Chem. Eng. J.* **140**(1–3), 32–42 (2008)
67. Sonal, S., Prakash, P., Mishra, B.K., Nayak, G.C.: Synthesis, characterization and sorption studies of a zirconium(IV) impregnated highly functionalized mesoporous activated carbons. *RSC Adv.* **10**(23), 13783–13798 (2020)
68. Chen, Z.X., Jin, X.Y., Chen, Z.L., Megharaj, M., Naidu, R.: Removal of methyl orange from aqueous solution using bentonite-supported nanoscale zero-valent iron. *J. Colloid. Interf. Sci.* **363**(2), 601–607 (2011)
69. Wu, C., Tu, J.W., Liu, W.Z., Zhang, J., Chu, S.Q., Lu, G.N., Lin, Z., Dang, Z.: The double influence mechanism of pH on arsenic removal by nano zero valent iron: electrostatic interactions and the corrosion of Fe⁰. *Environ. Sci.-Nano* **4**(7), 1544–1552 (2017)

70. Swiqtowski, A.: Surface area and porosity determinations by physisorption. Measurement, classical theories and quantum theory. *Przem. Chem.* **99**(5), 670–671 (2020)
71. An, L., Zhang, Z.Y., Feng, J.R., Lv, F., Li, Y.X., Wang, R., Lu, M., Gupta, R.B., Xi, P.X., Zhang, S.: Heterostructure-promoted oxygen electrocatalysis enables rechargeable zinc-air battery with neutral aqueous electrolyte. *J. Am. Chem. Soc.* **140**(50), 17624–17631 (2018)
72. Yu, H.J., Shang, L., Bian, T., Shi, R., Waterhouse, G.I.N., Zhao, Y.F., Zhou, C., Wu, L.Z., Tung, C.H., Zhang, T.R.: Nitrogen-doped porous carbon nanosheets templated from g-C₃N₄ as metal-free electrocatalysts for efficient oxygen reduction reaction. *Adv. Mater.* **28**(25), 5080–5086 (2016)
73. Wen, Z.H., Ci, S.Q., Zhang, F., Feng, X.L., Cui, S.M., Mao, S., Luo, S.L., He, Z., Chen, J.H.: Nitrogen-enriched core-shell structured Fe/Fe₃C-C nanorods as advanced electrocatalysts for oxygen reduction reaction. *Adv. Mater.* **24**(11), 1399–1404 (2012)
74. Wang, Z.L., Xiao, S., Zhu, Z.L., Long, X., Zheng, X.L., Lu, X.H., Yang, S.H.: Cobalt-embedded nitrogen doped carbon nanotubes: a bifunctional catalyst for oxygen electrode reactions in a wide pH range. *ACS Appl. Mater. Interf.* **7**(7), 4048–4055 (2015)
75. Yan, B., Concannon, N.M., Milshtein, J.D., Brushett, F.R., Surendranath, Y.: A membrane-free neutral pH formate fuel cell enabled by a selective nickel sulfide oxygen reduction catalyst. *Angew Chem. Int. Edit.* **56**(26), 7496–7499 (2017)
76. Liu, Y.H., Wang, X.K., Zhao, B.L., Shao, X., Huang, M.H.: Fe/Fe₃C nanoparticles encapsulated in N-doped hollow carbon spheres as efficient electrocatalysts for the oxygen reduction reaction over a wide pH range. *Chem.-Eur. J.* **25**(41), 9650–9657 (2019)
77. Tang, H.L., Zeng, Y., Zeng, Y.X., Wang, R., Cai, S.C., Liao, C., Cai, H.P., Lu, X.H., Tsiakaras, P.: Iron-embedded nitrogen doped carbon frameworks as robust catalyst for oxygen reduction reaction in microbial fuel cells. *Appl. Catal. B-Environ.* **202**, 550–556 (2017)
78. Santoro, C., Rojas-Carbonell, S., Awais, R., Gokhale, R., Kodali, M., Serov, A., Artyushkova, K., Atanassov, P.: Influence of platinum group metal-free catalyst synthesis on microbial fuel cell performance. *J. Power Sources.* **375**, 11–20 (2018)
79. Lv, C.C., Liang, B.L., Zhong, M., Li, K.X., Qi, Y.Y.: Activated carbon-supported multi-doped graphene as high-efficient catalyst to modify air cathode in microbial fuel cells. *Electrochim. Acta* **304**, 360–369 (2019)
80. Karaman, C.: Orange peel derived-nitrogen and sulfur co-doped carbon dots: a nano-booster for enhancing ORR electrocatalytic performance of 3D graphene networks. *Electroanalysis* **33**(5), 1356–1369 (2021)
81. Sethuraman, V.A., Weidner, J.W.: Analysis of sulfur poisoning on a PEM fuel cell electrode. *Electrochim. Acta* **55**(20), 5683–5694 (2010)
82. Santoro, C., Serov, A., Villarrubia, C.W.N., Stariha, S., Babanova, S., Artyushkova, K., Schuler, A.J., Atanassov, P.: High catalytic activity and pollutants resistivity using Fe-AAPyr cathode catalyst for microbial fuel cell application. *Sci. Rep.-UK* (2015). <https://doi.org/10.1038/srep16596>

Publisher's Note Springer Nature remains neutral with regard to jurisdictional claims in published maps and institutional affiliations.

Authors and Affiliations

Hassan Karimi-Maleh¹ · Ceren Karaman²  · Onur Karaman³ · Fatemeh Karimi⁴ · Yasser Vasseghian¹³ · Li Fu⁵ · Mehdi Baghayeri⁶ · Jalal Rouhi⁷ · P. Senthil Kumar⁸ · Pau-Loke Show⁹ · Saravanan Rajendran¹⁰ · Afsaneh L. Sanati¹¹ · Ali Mirabi¹²

✉ Hassan Karimi-Maleh
h.karimi.maleh@gmail.com

✉ Ceren Karaman
cerenkaraman@akdeniz.edu.tr

¹ School of Resources and Environment, University of Electronic Science and Technology of China, Xiyuan Ave, P.O. Box 611731, Chengdu, People's Republic of China

² Department of Electricity and Energy, Akdeniz University, Akdeniz University, Antalya 07070, Turkey

³ Department of Medical Imaging Techniques, Akdeniz University, Akdeniz University, Antalya 07070, Turkey

⁴ Department of Chemical Engineering, Quchan University of Technology, 9477177870 Quchan, Iran

⁵ College of Materials and Environmental Engineering, Hangzhou Dianzi University, Hangzhou 310018, People's Republic of China

⁶ Department of Chemistry, Faculty of Science, Hakim Sabzevari University, P.O. Box 397, Sabzevar, Iran

⁷ Faculty of Physics, University of Tabriz, 51566 Tabriz, Iran

⁸ Department of Chemical Engineering, Sri Sivasubramaniya Nadar College of Engineering, Kalavakkam, Chennai 603110, India

⁹ Department of Chemical and Environmental Engineering, Faculty of Science and Engineering, University of Nottingham Malaysia, Jalan Broga, 43500 Semenyih, Selangor Darul Ehsan, Malaysia

¹⁰ Faculty of Engineering, Department of Mechanical Engineering, University of Tarapaca, 1775 Arica, Chile

¹¹ Institute of Systems and Robotics, Department of Electrical and Computer Engineering, University of Coimbra, Polo II, 3030-290 Coimbra, Portugal

¹² Department of Chemistry, Qaemshahr Branch, Islamic Azad University, Qaemshahr, Iran

¹³ Department of Chemistry, Soongsil University, Seoul 06978, South Korea

